Geophysical Research Letters

RESEARCH LETTER
10.1029/2024GL108866

Global Ocean Cooling of 2.3°C During the Last Glacial Maximum

A. M. Seltzer[1], P. W. Davidson[1,2], S. A. Shackleton[1,3], D. P. Nicholson[1], and S. Khatiwala[4]

[1]Woods Hole Oceanographic Institution, Woods Hole, MA, USA, [2]Massachussetts Institute of Technology, Cambridge, MA, USA, [3]Princeton University, Princeton, NJ, USA, [4]University of Oxford, Oxford, UK

Abstract Quantitative constraints on past mean ocean temperature (MOT) critically inform our historical understanding of Earth's energy balance. A recently developed MOT proxy based on paleoatmospheric Xe, Kr, and N_2 ratios in ice core air bubbles is a promising tool rooted in the temperature dependences of gas solubilities. However, these inert gases are systematically undersaturated in the modern ocean interior, and it remains unclear how air-sea disequilibrium may have changed in the past. Here, we carry out 30 tracer-enabled model simulations under varying circulation, sea ice cover, and wind stress regimes to evaluate air-sea disequilibrium in the Last Glacial Maximum (LGM) ocean. We find that undersaturation of all three gases was likely reduced, primarily due to strengthened high-latitude winds, biasing reconstructed MOT by −0.38 ± 0.37°C (1σ). Accounting for air-sea disequilibrium, paleoatmospheric inert gases indicate that LGM MOT was 2.27 ± 0.46°C (1σ) colder than the pre-industrial era.

Plain Language Summary The ocean plays a central role in Earth's climate system as a major reservoir of heat. Understanding how ocean heat content (OHC) changed in the past is therefore key to unraveling the history of global climate. Xenon, krypton, and nitrogen trapped in ice core air bubbles offer a means of reconstructing past OHC, because changes in global ocean temperature affect the solubilities of these gases in seawater, leading to corresponding changes in their atmospheric abundances. For example, a colder ocean can hold more xenon, meaning less xenon resides in the atmosphere. However, these gases in the ocean today are slightly out of equilibrium with the atmosphere (i.e., they are undersaturated), and it remains unclear to what extent this disequilibrium could have changed in the past. We carried out global atmosphere-ocean model simulations, finding that undersaturation was likely reduced in the Last Glacial Maximum (LGM), a colder era of global climate ~20,000 years ago. Our analysis suggests that a small component of the additional xenon in the colder LGM ocean arose from this change in air-sea disequilibrium. After accounting for this effect, ice core noble gas measurements suggest a slightly warmer LGM ocean than previously thought.

A. M. Seltzer and P. W. Davidson contributed equally to this work.

Key Points:

- Global ocean air-sea gas exchange simulations suggest reduced undersaturation of inert gases in the Last Glacial Maximum (LGM) ocean
- Reduced LGM undersaturation indicates a small cold bias in mean ocean temperature (MOT) reconstruction from ice core noble gases
- A revised estimate of MOT, accounting for air-sea disequilibrium, is 2.27 ± 0.46°C colder than the pre-industrial era

Supporting Information:

Supporting Information may be found in the online version of this article.

Correspondence to:

A. M. Seltzer,
aseltzer@whoi.edu

Citation:

Seltzer, A. M., Davidson, P. W., Shackleton, S. A., Nicholson, D. P., & Khatiwala, S. (2024). Global ocean cooling of 2.3°C during the Last Glacial Maximum. *Geophysical Research Letters*, *51*, e2024GL108866. https://doi.org/10.1029/2024GL108866

Received 20 FEB 2024
Accepted 16 APR 2024

Author Contributions:

Conceptualization: A. M. Seltzer, S. A. Shackleton, D. P. Nicholson, S. Khatiwala
Data curation: A. M. Seltzer, P. W. Davidson, S. A. Shackleton
Formal analysis: A. M. Seltzer, P. W. Davidson
Funding acquisition: A. M. Seltzer, S. A. Shackleton, D. P. Nicholson, S. Khatiwala

1. Introduction

With a heat capacity three orders of magnitude larger than the atmosphere, the ocean plays a leading role in modulating Earth's surface temperature. The global ocean has taken up over 90% of the excess heat in the Earth system since the Industrial Revolution (Cheng et al., 2017; Levitus et al., 2012; Zanna et al., 2019), and ocean heat uptake accounts for roughly half of the total planetary energy gain during the Last Glacial Termination (~18–11 ka) (Baggenstos et al., 2019). Robustly quantifying past changes in ocean heat content (OHC) is therefore crucial for understanding long-term changes in Earth's energy balance. The recent development of an ice core proxy for mean ocean temperature (MOT), based on past changes in the relative abundance of inert gases in the well-mixed troposphere, represents a major advance toward precisely constraining past OHC changes. Of particular climatic interest is the change in OHC during the Last Glacial Maximum (LGM, ~26–18 ka), when global surface temperatures were cooler (Seltzer et al., 2021; Tierney et al., 2020), atmospheric CO_2 concentrations were reduced (Marcott et al., 2014), sea level was lower (Lambeck et al., 2014), and ocean circulation was altered (Curry & Oppo, 2005).

The ice-core MOT proxy makes use of the different solubility temperature dependency of Xe, Kr, and N_2 in seawater (Hamme & Emerson, 2004; Jenkins et al., 2019) to infer past MOT based on ice core measurements of past atmospheric composition. The underlying principle is that cooling enhances gas solubilities in the global ocean, leading to a net transfer of inert gases from the atmosphere to ocean, with the relative effect being largest for Xe (most temperature sensitive) and smallest for N_2 (least temperature sensitive). As the inventories of inert

Investigation: A. M. Seltzer, P. W. Davidson
Methodology: A. M. Seltzer, P. W. Davidson, S. A. Shackleton, D. P. Nicholson, S. Khatiwala
Project administration: A. M. Seltzer
Resources: A. M. Seltzer, D. P. Nicholson, S. Khatiwala
Software: A. M. Seltzer, P. W. Davidson, D. P. Nicholson, S. Khatiwala
Supervision: A. M. Seltzer, D. P. Nicholson
Validation: A. M. Seltzer, P. W. Davidson, S. A. Shackleton, D. P. Nicholson, S. Khatiwala
Visualization: A. M. Seltzer
Writing – original draft: A. M. Seltzer
Writing – review & editing: A. M. Seltzer, P. W. Davidson, S. A. Shackleton, D. P. Nicholson, S. Khatiwala

gases are conserved within the ocean-atmosphere system, differential changes in global ocean gas content (e.g., between Xe and N_2) will impact atmospheric gas ratios. For example, cooling of the global ocean will lower the atmospheric Xe/N_2 ratio because a greater fraction of atmospheric Xe, relative to N_2, is transferred to the ocean. A recent compilation of ice core inert gas measurements (Shackleton et al., 2023) from three Antarctic ice cores (Baggenstos et al., 2019; Bereiter et al., 2018; Shackleton et al., 2019, 2020) precisely constrains the change in Xe/N_2, Kr/N_2, and Xe/Kr in the LGM atmosphere to -3.23 ± 0.36‰, -1.15 ± 0.17‰, and -2.07 ± 0.29‰ (1σ), respectively, relative to the modern atmosphere, as shown in Figure S1 in Supporting Information S1. The corresponding change in MOT based on these inert gas constraints is -2.65 ± 0.27°C (1σ) relative to the pre-industrial ocean, if changes in air-sea disequilibrium are neglected (Shackleton et al., 2023).

Although the MOT proxy is conceptually based on the temperature dependency of equilibrium solubility functions, concentrations of Xe, Kr, and N_2 in the modern ocean are not in perfect solubility equilibrium with the atmosphere. Each of these gases displays a characteristic undersaturation in the deep ocean of up to several percent that is largest for Xe and smallest for N_2. Prior studies have attributed these disequilibria to rapid cooling in association with deep water formation, incomplete equilibration, and bubble injection from breaking waves and/or the release of occluded air bubbles during submarine glacial ice melting (Hamme & Severinghaus, 2007; Hamme et al., 2017; Jenkins et al., 2016, 2023; Loose & Jenkins, 2014; Loose et al., 2016; Seltzer et al., 2019, 2023). These processes have also been linked to the kinetics of global atmosphere-ocean disequilibria and corresponding fluxes of chlorofluorocarbons, CO_2, and O_2 (Keeling et al., 1998; Takahashi et al., 1997; Wang et al., 2021). A recent study suggested that changes in the magnitude of air-sea disequilibria in the LGM ocean could have an appreciable effect on paleoatmospheric inert gas ratios, raising the possibility that previous ice-core based MOT estimates—which have not accounted for changes in air-sea disequilibrium—could be biased (Pöppelmeier et al., 2023). Thus, for example, a reduction in air-sea disequilibrium in the LGM ocean could increase the ocean inventory of Xe and thereby reduce atmospheric Xe/N_2 independent of ocean cooling, leading to a cold bias in ice-core estimates of MOT.

Here we carry out a suite of 30 tracer-enabled ocean general circulation model (GCM) experiments to simulate the solubility disequilibria of Xe, Kr, and N_2 in the LGM ocean. Using the results of these simulations, we assess the likely impact of past changes in air-sea exchange on paleoatmospheric inert gas ratios and corresponding inferences of MOT. Finally, we discuss the physical mechanisms underlying these simulated changes and present a revised estimate and uncertainty range for LGM MOT change.

2. Model Simulations of Air-Sea Disequilibrium in the LGM Ocean

To estimate changes in solubility disequilibria, we simulated physical air-sea gas exchange and transport of gases within the ocean interior. We define solubility disequilibrium, Δ_{eq}, for a dissolved gas as

$$\Delta_{eq} \equiv \left(\frac{C}{C_{eq}} - 1\right) \times 100 \quad (1)$$

where C is the concentration of a gas (Xe, Kr, or N_2) in a parcel of seawater and C_{eq} is the equilibrium concentration of that gas at the potential temperature and salinity of the water parcel at global-mean sea level pressure (SLP) (e.g., 1 atm in the present day).

The primary goal of this study is to determine sensitivities of global volume-weighted mean Δ_{eq} of Xe, Kr, and N_2 (see Text S1 in Supporting Information S1) to different ocean properties (e.g., circulation, temperature, salinity, sea ice, wind stress) relative to a pre-industrial control (PIC) experiment through a suite of model simulations. Table S1 in Supporting Information S1 summarizes the details and results from 30 simulations, each of which was carried out using the UVic Earth System Climate Model (UVic ESCM; Weaver et al., 2010), which has a 1.8° latitude × 3.6° longitude grid with 19 vertical ocean layers. Climatological surface wind fields from Coordinated Ocean Research Experiments version 2 (CORE-2) (Large & Yeager, 2022) at 6 hourly resolution were used, with windspeed enhanced or diminished by up to 50% in the high latitudes (poleward of 50°) across these experiments (Table S1 in Supporting Information S1). The physical transport of dissolved gas tracers within the ocean is performed offline using the transport matrix method (TMM; Khatiwala, 2007; Khatiwala, 2018) run to steady state (8,000 years) in each experiment.

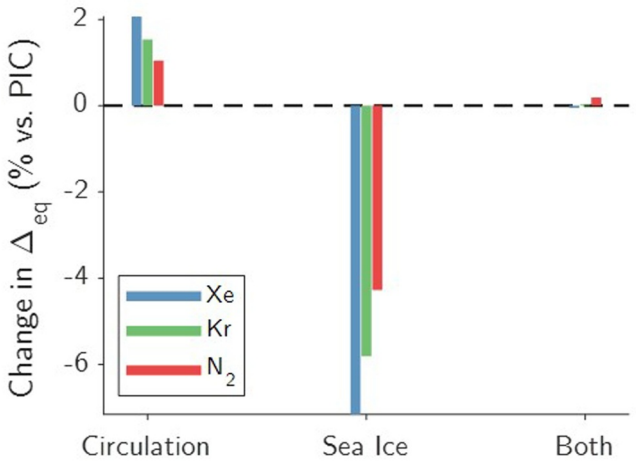

Figure 1. Influence of Last Glacial Maximum (LGM) circulation and sea ice on mean-ocean gas saturation anomalies, Δ_{eq}. Changes in Δ_{eq} are shown for Xe, Kr, and N_2 by comparing three equilibrium simulation experiments to the pre-industrial control (PIC) simulation: (1) Circulation: LGM circulation with PIC winds and sea ice; (2) Sea Ice: LGM sea ice with PIC winds and circulation; (3) Both: LGM sea ice and circulation with PIC winds. The individual variable experiments are useful in a diagnostic sense, demonstrating that slower/shallower LGM circulation acts to reduce undersaturation (increase Δ_{eq}) and enhanced LGM sea ice extent acts to increase undersaturation (reduce Δ_{eq}). The individual effects are non-additive–i.e., simultaneously changing both circulation and sea ice to LGM conditions results in virtually no change in Δ_{eq}, despite the different magnitudes of Δ_{eq} responses to single-forcing experiments.

Model experiments were carried out with transport matrices extracted from the PIC and LGM configurations of UVic ESCM constrained by an extensive set of modern oceanographic and sedimentary paleoproxy observations (Khatiwala et al., 2019; Muglia & Schmittner, 2015). Depending on the experiment, sea ice fields were prescribed using either the corresponding PIC or LGM UVic simulation, or an enhanced LGM sea ice field (equatorward shift of 1.8°) as shown in Figures S2–S4 in Supporting Information S1. Air-sea gas exchange was simulated using a bubble-mediated parameterization (Liang et al., 2013), and gas fluxes were scaled down linearly by sea ice area fraction (e.g., no gas exchange occurs in a fully sea ice-covered grid cell). Imposed wind speed changes in our experiments directly influence gas exchange, but not circulation, which is separately prescribed from LGM or PIC transport matrices. Fifteen sets of identical sets of simulations were carried out implementing either the original model (L13b1) or a modification with enhanced bubble fluxes (L13b2). The latter has recently been shown to better reproduce a set of high-precision inert gas tracer measurements in the modern ocean (Seltzer et al., 2023). Global-mean Δ_{eq} results for the L13b2 PIC simulation were −3.2%, −2.3%, and −0.4% for Xe, Kr, and N_2, respectively, closely resembling a recent compilation of global noble gas and N_2 measurements (Hamme et al., 2018). Whereas global-mean Δ_{eq} values were lower in the L13b1 PIC (−4.5%, −3.4%, and −1.7% for Xe, Kr, and N_2, respectively), simulated *changes* in Δ_{eq}, relative to their respective PIC simulations, across all experiments carried out in this study, were nearly identical between the L13b1 and L13b2 sets of simulations, with a root-mean-squared deviation of 0.1% or less for all gases (Figure S5 in Supporting Information S1). Because the goal of this study is to constrain such changes in Δ_{eq} between the LGM and pre-industrial era, this indicates that our analysis is insensitive to scaling of bubble fluxes. Hereafter, all results are from the L13b2 set of simulations.

We first consider separately the influences of sea ice and circulation on air-sea disequilibrium by holding near-surface (10 m) winds constant at PIC values. Figure 1 shows the results of three experiments implementing (a) LGM circulation with PIC sea ice and winds, (b) LGM sea ice with PIC circulation and winds, and (c) LGM circulation and sea ice with PIC winds. We find that slower overturning circulation in the LGM reduces undersaturation while sea ice enhances undersaturation (Khatiwala et al., 2019), with the effects being largest for Xe and smallest for N_2. Crucially, we find that circulation and sea ice effects are not additive, as was previously found for dissolved inorganic carbon and oxygen (Cliff et al., 2021; Khatiwala et al., 2019), and that simultaneously replacing PIC circulation and sea ice with LGM fields leads to virtually no change in Δ_{eq} (−0.05%, +0.03%, +0.19% for Xe, Kr, and N_2, respectively). The lack of change in Δ_{eq} reflects compensation between a reduced driving forcing toward disequilibrium (i.e., reduced sea-to-air heat flux in a more sluggish ocean) and a reduced restoring force toward equilibrium (i.e., impedance of gas transfer by sea ice). A separate analysis of experiments carried out with fixed LGM circulation but either PIC, LGM, or expanded LGM sea ice confirm that sea ice extent, by itself, acts to enhance undersaturation (Figure S6 in Supporting Information S1). Given a lack of quantitative knowledge about the extent of LGM sea ice, we adopt half the differences in Δ_{eq} between LGM circulation experiments with LGM and PIC sea ice (Figures S2 and S3 in Supporting Information S1) as an estimate of the 1σ uncertainty in Δ_{eq} associated with sea ice extent.

To assess the role of changes in high-latitude near-surface winds in the LGM, considering the non-additivity of sea ice and circulation effects, we carried out a set of simulations implementing both LGM circulation and LGM sea ice while enhancing or diminishing high-latitude wind speed (poleward of 50°) relative to the PIC. Figure 2 shows the results of these simulations, indicating that strengthened winds act to reduce undersaturation, while weakened winds act to increase undersaturation of Xe, Kr, and N_2. Enhancement of undersaturation induced by weaker winds is largest for Xe, whereas reduction of undersaturation by stronger winds is largest for N_2. Of these three gases, Xe is the slowest diffusing, most soluble, and most temperature dependent (in terms of its solubility). Reducing wind speed slows gas exchange, allowing a larger cooling-induced undersaturation to persist without

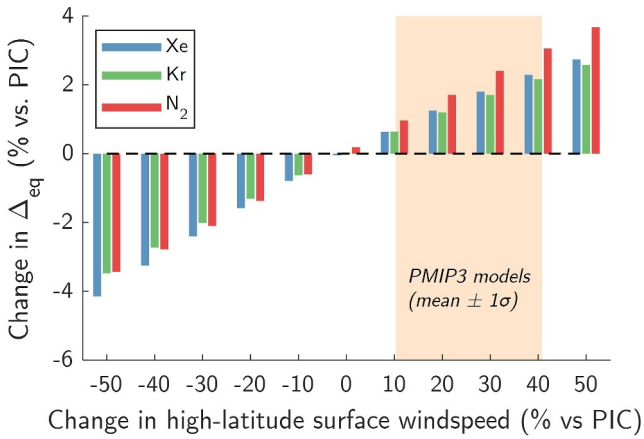

Figure 2. Influence of changes in high-latitude surface windspeed on mean-ocean gas saturation anomalies, Δ_{eq}. In each equilibrium simulation experiment above, mean-annual surface windspeed at high latitudes (poleward of 50°) are enhanced or diminished relative to the pre-industrial control (PIC) simulation, and Last Glacial Maximum (LGM) ocean circulation and sea ice fields are implemented. The shaded region reflects Paleoclimate Modeling Intercomparison Project modeled high-latitude wintertime (DJF in NH; JJA in SH) surface wind speed change between LGM and PIC experiments (inter-model mean ± 1σ; Table S2 in Supporting Information S1).

erasure by air-to-sea gas transfer, which affects Xe undersaturation the most. Conversely, increasing wind speed enhances air-to-sea gas transfer due to faster surface diffusion and enhanced bubble fluxes (both injection of completely dissolving bubbles and exchange across partially dissolving bubbles). This reduces or eliminates the undersaturation caused by cooling of the high-latitude surface ocean, the effect being largest for N_2, because it is the least soluble and thus most sensitive to bubble injection (Hamme & Emerson, 2004, 2013). While Kr and Xe are less sensitive to injection of completely dissolving bubbles, wind-driven bubble fluxes still enhance gas exchange across partially dissolving bubbles, which reduces or eliminates cooling-driven undersaturation. Recent Ar isotope constraints in the modern ocean suggest that enhanced exchange of heavier noble gases across partially dissolving bubbles is an important process (Seltzer et al., 2023).

Although considerable uncertainty exists regarding high-latitude near-surface wind speed in the LGM, particularly in the Southern Ocean, numerous proxy and model-based studies suggest strengthened winds in the LGM (Kohfeld et al., 2013; McGee et al., 2010; Moore et al., 2000; Sime et al., 2013, 2016). Other studies indicate a mean LGM weakening of the Antarctic Circumpolar Current and westerly winds (Gray et al., 2023; Lamy et al., 2015). Deep water formation and ventilation of the interior ocean is largely a winter phenomenon, and, to our knowledge, there are no proxy constraints on wintertime wind speed changes in the high northern and southern latitude regions of deep water formation in the LGM. Thus, we analyzed LGM-PIC wind speed changes in the third generation of Paleoclimate Modeling Intercomparison Project (PMIP3), the most recent era with available climatological wind fields. Following the change in ocean water mass volumes suggested by Bereiter et al. (2018), we assume that roughly one third of the global ocean is ventilated by the wintertime high northern latitudes and two thirds by the wintertime high southern latitudes. The intermodel mean increase in high-latitude winds (poleward of 50°) is 25.6 ± 15.3% (1σ), based on PMIP3 models (Table S2 in Supporting Information S1; Adloff et al., 2018; Brady et al., 2013; Kageyama, Braconnot, Bopp, Caubel, et al., 2013; Kageyama, Braconnot, Bopp, Mariotti, et al., 2013; Sueyoshi et al., 2013; Voldoire et al., 2013; Yukimoto et al., 2012; Zheng & Yu, 2013). As an alternate test, we identified regions of deep-water formation based on UVic mixed layer depth anomalies (Figure S7 in Supporting Information S1) and calculated LGM-PIC changes in wind speed over these regions, finding a virtually identical result of 22.8 ± 18.4% (1σ; Table S2 in Supporting Information S1). Adopting the PMIP3 high-latitude LGM-PIC change in near-surface wind speed, our air-sea gas exchange simulations suggest mean changes in Δ_{eq} of Xe, Kr, and N_2 of +1.51% (68% CI: +0.13 to +2.83%), +1.44% (68% CI: +0.34 to +2.50%), and +2.02% (68% CI: +0.85 to +3.18%), respectively, in the LGM ocean.

3. Non-Temperature Effects on LGM Atmospheric Gas Ratios and Inferred MOT

A reduction of undersaturation in the LGM ocean (i.e., an increase in Δ_{eq}) implies that the ocean held a larger fraction of the total ocean-atmosphere inventory of each these inert gases than would be expected if Δ_{eq} were constant in time. The sensitivity of an atmospheric gas ratio to changes in global air-sea disequilibrium is strongly controlled by the change in Δ_{eq} of the more soluble gas, since a larger fraction of its total ocean-atmosphere inventory resides in the ocean. In other words, because ∼5% of global Xe–but only ∼0.5% of global N_2–resides in the ocean, an equal magnitude increase in Δ_{eq} of both Xe and N_2 would act to decrease the atmospheric Xe/N_2 ratio. A decrease in atmospheric Xe/N_2 due entirely to changes in global air-sea disequilibrium (i.e., independent of changes in LGM MOT) would impart a cold bias on ice-core Xe/N_2-based estimates of MOT that assume no change in Δ_{eq} over time. Figure 3 illustrates this effect, showing how changes in Δ_{eq} of Xe and N_2 influence both the atmospheric Xe/N_2 ratio and corresponding estimates of MOT (Figures S8 and S9 in Supporting Information S1 show equivalent effects for atmospheric Kr/N_2 and Xe/Kr ratios.). Hereafter, we refer to biases (relative to the assumption of constant Δ_{eq}) in atmospheric ratios and MOT due to changes in air-sea disequilibrium as δ' and $\Delta MOT'$, respectively.

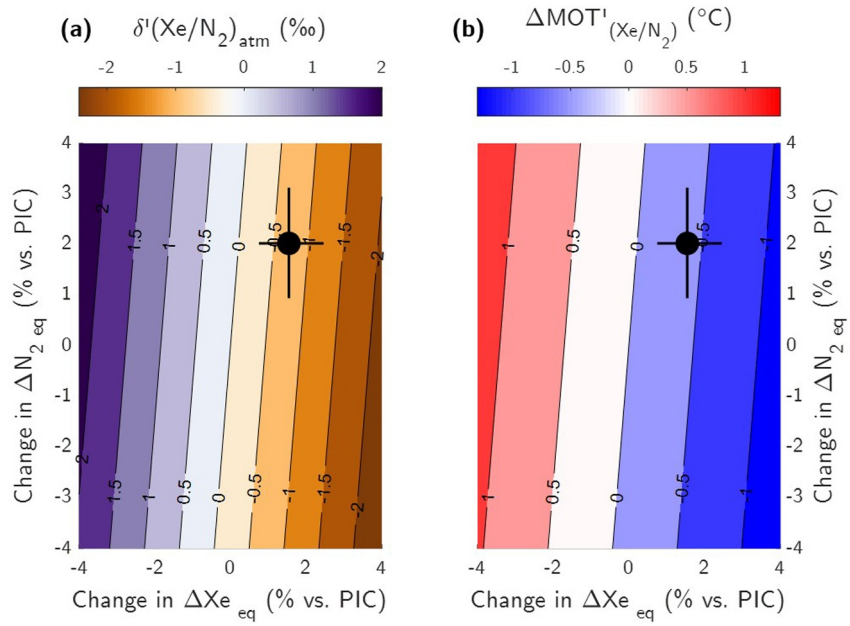

Figure 3. Biases in panel (a) Last Glacial Maximum (LGM) atmospheric Xe/N_2 ratio, $\delta'(Xe/N_2)_{atm}$, and (b) corresponding LGM mean-ocean temperature ($\Delta MOT'$) arising from (unaccounted-for) changes in mean-ocean gas saturation anomalies, Δ_{eq}. Black markers and error bars refer to the mean and standard deviation of simulated LGM changes in Δ_{eq} in this study.

To estimate LGM δ' and $\Delta MOT'$, we carried out 10^6 Monte Carlo simulations (see Text S2 in Supporting Information S1) in which simulated LGM changes in Δ_{eq} (Section 2) lead to changes in the partitioning of inert gases between the LGM atmosphere and ocean. For example, an LGM increase in Δ_{eq} for a particular gas would increase the ocean inventory and decrease the atmospheric inventory of that gas. Thus, for changes in Δ_{eq}, we calculate corresponding changes in atmospheric gas ratios (δ') and their implied MOT bias ($\Delta MOT'$). These Monte Carlo simulations also account for regional changes in SLP over the glacial ocean, as some of the apparent air-sea disequilibrium (Δ_{eq}) of the modern ocean is attributable to the fact that the high-latitude regions of ocean ventilation are characterized by persistent low SLP anomalies (Allan & Ansell, 2006). We define anomalies high-latitude wintertime SLP relative to global-mean SLP as ΔP_{HL} (e.g., ΔP_{HL} is $\sim -2\%$, or ~ -20 mbar, in the present) and include PMIP3-based changes in LGM ΔP_{HL} (relative to the PIC) in the Monte Carlo analysis. The PMIP3 intermodel mean LGM-PI change in ΔP_{HL} is $-0.2 \pm 0.2\%$ (1σ), indicating a slight deepening of high-latitude low SLP systems in the LGM (Table S3 in Supporting Information S1). This leads to a small equal-parts reduction in the global ocean inventories of Xe, Kr, and N_2, because a change in SLP changes the sea-surface partial pressures—and thus equilibrium dissolved concentrations—of all three gases by the same fraction (Jenkins et al., 2024).

Figure 4 shows the results of this Monte Carlo analysis, which suggests median δ' values (and 68% CI) of $-0.70‰$ (-1.42 to $+0.05‰$), $-0.27‰$ (-0.52 to $-0.14‰$), and $-0.43‰$ (-0.90 to $+0.06‰$) for Xe/N_2, Kr/N_2, and Xe/Kr ratios, respectively. In other words, reduced LGM air-sea disequilibrium acts to lower all three atmospheric gas ratios, independent of a change in MOT. By adopting MOT sensitivities of 1.85 $‰°C^{-1}$, 0.71 $‰°C^{-1}$, and 1.14 $‰°C^{-1}$ (determined by perturbing the LGM ocean box model of Bereiter et al. (2018) by 1°C), each of these δ' values independently implies virtually the same $\Delta MOT'$ of -0.38°C (68% CI: -0.74 to -0.01°C). Approximating $\Delta MOT'$ as normally distributed and incorporating uncertainty estimates of Shackleton et al. (2023), which account for both analytical and systematic sources of uncertainty, this analysis suggests a revised LGM MOT of -2.27 ± 0.46°C, relative to the pre-industrial era ocean. This uncertainty estimate reflects the quadrature sum of uncertainties associated with random measurement errors, firn air corrections, and air-sea disequilibria.

4. Discussion

Our finding of a cold bias in LGM MOT is consistent with the findings of a recent modeling study that suggested a $\Delta MOT'$ value of -0.50 ± 0.67°C (Pöppelmeier et al., 2023). However, our analysis differs from Pöppelmeier

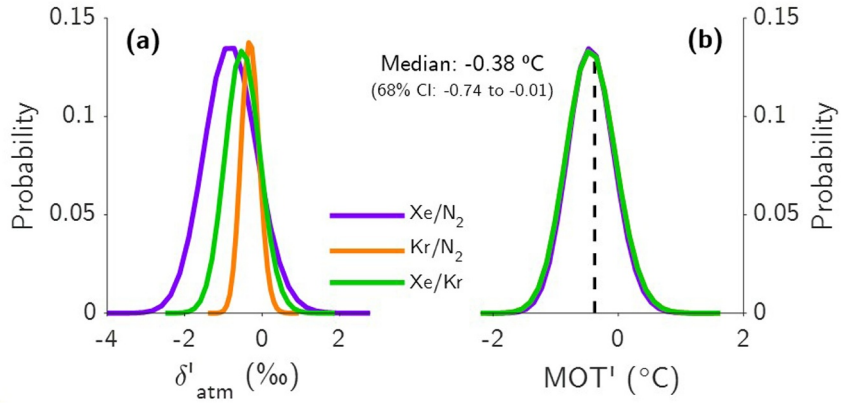

Figure 4. Probability distributions (based on 10^6 Monte Carlo simulations) for (a) biases in atmospheric gas ratios (δ') and (b) corresponding biases in reconstructed mean ocean temperature (MOT) (MOT′) that are determined from atmospheric gas ratios. This analysis suggests that reduced undersaturation in the Last Glacial Maximum (LGM) ocean acted to lower atmospheric Xe/N_2, Kr/N_2, and Xe/Kr, implying a median MOT bias of −0.38°C and corresponding revised optimal estimate for LGM MOT of −2.27 ± 0.46°C (±1σ).

et al. (2023) in several fundamental ways, providing an important and independent update for the ice core MOT proxy. Pöppelmeier et al. (2023) ran several air-sea gas exchange simulations, but could not reconcile their results with ice core noble gas data and constraints on LGM surface cooling. As a result, they ultimately adopted an MOT estimate based on the underlying GCM potential temperature, rather than ice core data or independent estimates of air-sea disequilibrium. Pöppelmeier et al. (2023) suggest that their findings are supported by an observed offset in reconstructed MOT from Kr/N_2 and Xe/N_2 for two ice cores, but they do not consider a third core (Shackleton et al., 2020, 2023) that displays the opposite offset. Notably, none of these Kr/N_2 versus Xe/N_2 offsets fall outside the reported uncertainty bounds. The mismatch of ice core data with the model of Pöppelmeier et al. (2023) led the authors to include a wide uncertainty estimate in noble gas disequilibria (translating to a 0.7°C error bar in MOT) and to call for future studies to revisit disequilibrium in the LGM.

Our approach offers an important update because it (a) ultimately relies on MOT constrained by ice core observations rather than a GCM, (b) includes all available LGM ice core constraints, and (c) indicates that changes in air-sea disequilibria of Xe, Kr, and N_2 likely occur in near-exact proportions to changes in MOT such that biases in MOT arising from air-sea disequilibria are virtually identical. That is, our estimates of MOT′ from Xe/N_2, Kr/N_2, and Xe/Kr all agree, on average, to within 0.01°C, serving as an important internal consistency check that provides additional confidence in our result.

One potential limitation of our analysis is that, because the effects of sea ice and circulation are nearly equal and opposite, changes in Δ_{eq} are predominantly controlled by high-latitude wind speed in the LGM, which is poorly constrained. While the PMIP inter-model mean and spread arguably represents the best available estimate of LGM wind speed and its uncertainty, if new constraints on LGM wind strength emerge in the future, our analysis would provide a useful scaling factor with which to update ice-core MOT estimates. That is, approximating the dependences of Δ_{eq} on high-latitude wind speed as linear (Figure 2), for a 10% increase in high-latitude wind speed in the LGM, the corresponding cold bias in MOT is ∼0.15°C. Thus, for example, if evidence were to emerge indicating that the mean LGM wintertime high-latitude wind speed change relevant for ocean ventilation was in fact +15% (instead of the +25.6% value adopted in this study), a corresponding revised estimate of LGM MOT would be ∼0.15°C colder.

Intriguingly, we find independent support for our revised estimate of MOT from the marine sedimentary record of benthic foraminiferal oxygen isotope ratios, which are a function of deep-sea temperature and ice volume. Shackleton et al. (2023) combined ice-core-based MOT with global sea-level reconstructions over the last deglaciation (Lambeck et al., 2014; Yokoyama et al., 2018) to estimate their equivalent contributions to global-mean benthic foraminifera $\delta^{18}O$ (Lisiecki & Stern, 2016). Using an ice-core-based MOT record that neglects changes in Δ_{eq}, Shackleton et al. (2023) found that reconstructed LGM $\delta^{18}O$ is higher than foraminifera observations by either 0.21 ± 0.17‰ or 0.08 ± 0.17‰, depending on whether the sea-level reconstruction of

Lambeck et al. (2014) or Yokoyama et al. (2018), respectively, is adopted. If we instead account for MOT bias using the median air-sea disequilibria found in this study, the combined sea-level/MOT estimate of benthic $\delta^{18}O$ more closely matches the benthic stack. In particular, the constant LGM offset of ~0.08‰ offset between the benthic stack and composite noble gas and Yokoyama et al. (2018) sea-level reconstruction found by Shackleton et al. (2023) is equivalent to −0.36°C, which virtually disappears when we apply the median −0.38°C cold bias suggested by our analysis. This provides key independent support for reduced undersaturation of noble gases in the LGM ocean. Additionally, our updated LGM MOT cooling estimate of 2.27 ± 0.46°C is in good agreement with a recent global deep-sea temperature reconstruction that found 2.5 ± 0.3°C of LGM cooling (Rohling et al., 2021), which marked a downward revision from a previous estimate of 3 ± 1°C (Elderfield et al., 2012).

5. Conclusions

In this study, we explored the solubility disequilibria of Xe, Kr, and N_2 in the LGM ocean by carrying out a suite of GCM experiments using an air-sea gas exchange framework validated by inert gas observations in the modern ocean. We find that slower meridional overturning circulation and enhanced sea ice in the LGM act to reduce and increase inert gas undersaturation, respectively, and that their combined effects cancel each other, leaving wintertime high-latitude near-surface wind speed as the primary driver of LGM changes in global ocean solubility disequilibria. While proxy evidence on the strength of southern high-latitude winds in the LGM is mixed, simulations from the Paleo Model Intercomparison Project indicate enhanced wind speeds in both the northern and southern high-latitude places (and seasons) of deep-water formation. Our analysis correspondingly suggests that inert gas undersaturation in the LGM ocean was likely reduced, leading to a lowering of atmospheric Xe/N_2, Kr/N_2, and Xe/Kr ratios. Future improvements in our understanding of high-latitude winds in the LGM will help to substantially reduce uncertainties in LGM MOT, in addition to providing insight into other important climate processes. Our analysis suggests a 0.38 ± 0.37°C (1σ) cold bias in LGM MOT (if changes in air-sea disequilibrium are neglected), reconciling ice-core based MOT with benthic foraminiferal oxygen isotope and sea level records. These records thus provide independent support for a revised LGM MOT estimate of −2.27 ± 0.46°C (1σ), relative to the preindustrial era ocean, which represents an important quantitative refinement to our understanding of past changes in planetary energy balance.

Data Availability Statement

- All data on which this article is based are available in Seltzer (2024): https://doi.org/10.5281/zenodo.10402435
- Code, transport matrices and forcing data required to perform the simulations are available in Khatiwala (2024): https://github.com/samarkhatiwala/tmm

Acknowledgments
We are grateful to the US National Science Foundation (Grant OPP, 2049359) and UK NERC (Grant NE/W007258/1) for supporting this work. Computing resources were provided by the Climate Simulation Laboratory at the National Center for Atmospheric Research Computational and Information Systems Laboratory (ark:/85065/d7wd3xhc), sponsored by the NSF and other agencies, and the University of Oxford Advanced Research Computing facility (https://doi.org/10.5281/zenodo.22558).

References

Adloff, M., Reick, C. H., & Claussen, M. (2018). Earth system model simulations show different feedback strengths of the terrestrial carbon cycle under glacial and interglacial conditions. *Earth System Dynamics*, *9*(2), 413–425. https://doi.org/10.5194/ESD-9-413-2018

Allan, R., & Ansell, T. (2006). A new globally complete monthly historical gridded mean sea level pressure dataset (HadSLP2): 1850–2004. *Journal of Climate*, *19*(22), 5816–5842. https://doi.org/10.1175/JCLI3937.1

Baggenstos, D., Häberli, M., Schmitt, J., Shackleton, S. A., Birner, B., Severinghaus, J. P., et al. (2019). Earth's radiative imbalance from the Last Glacial Maximum to the present. *Proceedings of the National Academy of Sciences of the United States of America*, *116*(30), 14881–14886. https://doi.org/10.1073/pnas.1905447116

Bereiter, B., Shackleton, S., Baggenstos, D., Kawamura, K., & Severinghaus, J. (2018). Mean global ocean temperatures during the last glacial transition. *Nature*, *553*(7686), 39–44. https://doi.org/10.1038/nature25152

Brady, E. C., Otto-Bliesner, B. L., Kay, J. E., & Rosenbloom, N. (2013). Sensitivity to glacial forcing in the CCSM4. *Journal of Climate*, *26*(6), 1901–1925. https://doi.org/10.1175/JCLI-D-11-00416.1

Cheng, L., Trenberth, K. E., Fasullo, J., Boyer, T., Abraham, J., & Zhu, J. (2017). Improved estimates of ocean heat content from 1960 to 2015. *Science Advances*, *3*(3), e1601545. https://doi.org/10.1126/sciadv.1601545

Cliff, E., Khatiwala, S., & Schmittner, A. (2021). Glacial deep ocean deoxygenation driven by biologically mediated air–sea disequilibrium. *Nature Geoscience*, *14*(1), 43–50. https://doi.org/10.1038/s41561-020-00667-z

Curry, W. B., & Oppo, D. W. (2005). Glacial water mass geometry and the distribution of δ13C of ΣCO2 in the western Atlantic Ocean. *Paleoceanography*, *20*(1). https://doi.org/10.1029/2004PA001021

Elderfield, H., Ferretti, P., Greaves, M., Crowhurst, S., McCave, I. N., Hodell, D., & Piotrowski, A. M. (2012). Evolution of ocean temperature and ice volume through the mid-pleistocene climate transition. *Science*, *337*(6095), 704–709. https://doi.org/10.1126/science.1221294

Gray, W. R., de Lavergne, C., Jnglin Wills, R. C., Menviel, L., Spence, P., Holzer, M., et al. (2023). Poleward shift in the southern hemisphere westerly winds synchronous with the deglacial rise in CO2. *Paleoceanography and Paleoclimatology*, *38*(7), e2023PA004666. https://doi.org/10.1029/2023PA004666

Hamme, R. C., & Emerson, S. R. (2004). The solubility of neon, nitrogen and argon in distilled water and seawater. *Deep-Sea Research Part I Oceanographic Research Papers*, *51*(11), 1517–1528. https://doi.org/10.1016/j.dsr.2004.06.009

Hamme, R. C., & Emerson, S. R. (2013). Deep-sea nutrient loss inferred from the marine dissolved N2/Ar ratio. *Geophysical Research Letters*, *40*(6), 1149–1153. https://doi.org/10.1002/GRL.50275

Hamme, R. C., Emerson, S. R., Severinghaus, J. P., Long, M. C., & Yashayaev, I. (2017). Using noble gas measurements to derive air-sea process information and predict physical gas saturations. *Geophysical Research Letters*, *44*(19), 9901–9909. https://doi.org/10.1002/2017GL075123

Hamme, R. C., Jenkins, W. J., Emerson, S. R., & Nicholson, D. P. (2018). A compilation of dissolved noble gas and N2/Ar ratio measurements collected from 1999–2016 in locations spanning the globe. https://doi.org/10.1575/1912/bco-dmo.744563

Hamme, R. C., & Severinghaus, J. P. (2007). Trace gas disequilibria during deep-water formation. *Deep-Sea Research Part I Oceanographic Research Papers*, *54*(6), 939–950. https://doi.org/10.1016/j.dsr.2007.03.008

Jenkins, W. J., Doney, S. C., Seltzer, A. M., German, C. R., Lott, D. E., & Cahill, K. L. (2023). A North Pacific meridional section (U.S. GEOTRACES GP15) of helium isotopes and noble gases I: Deep water distributions. *Global Biogeochemical Cycles*, *37*(5). https://doi.org/10.1029/2022GB007667

Jenkins, W. J., Lott, D. E., & Cahill, K. L. (2019). A determination of atmospheric helium, neon, argon, krypton, and xenon solubility concentrations in water and seawater. *Marine Chemistry*, *211*, 94–107. https://doi.org/10.1016/j.marchem.2019.03.007

Jenkins, W. J., Lott, D. E., German, C. R., Cahill, K. L., Goudreau, J., & Longworth, B. (2016). The deep distributions of helium isotopes, radiocarbon, and noble gases along the U.S. GEOTRACES East Pacific Zonal Transect (GP16). *Marine Chemistry*, *201*, 167–182. https://doi.org/10.1016/j.marchem.2017.03.009

Jenkins, W. J., Seltzer, A. M., Gebbie, G., & German, C. R. (2024). Noble gas evidence of a millennial-scale deep North Pacific palaeo-barometric anomaly. *Nature Geoscience*, *17*(2), 1–4. https://doi.org/10.1038/s41561-023-01368-z

Kageyama, M., Braconnot, P., Bopp, L., Caubel, A., Foujols, M.-A., Guilyardi, E., et al. (2013). Mid-holocene and Last Glacial Maximum climate simulations with the IPSL model—Part I: Comparing IPSL_CM5A to IPSL_CM4. *Climate Dynamics*, *40*(9), 2447–2468. https://doi.org/10.1007/s00382-012-1488-8

Kageyama, M., Braconnot, P., Bopp, L., Mariotti, V., Roy, T., Woillez, M.-N., et al. (2013). Mid-holocene and last glacial maximum climate simulations with the IPSL model: Part II: Model-data comparisons. *Climate Dynamics*, *40*(9), 2469–2495. https://doi.org/10.1007/s00382-012-1499-5

Keeling, R. F., Stephens, B. B., Najjar, R. G., Doney, S. C., Archer, D., & Heimann, M. (1998). Seasonal variations in the atmospheric O2/N2 ratio in relation to the kinetics of air-sea gas exchange. *Global Biogeochemical Cycles*, *12*(1), 141–163. https://doi.org/10.1029/97GB02339

Khatiwala, S. (2007). A computational framework for simulation of biogeochemical tracers in the ocean. *Global Biogeochemical Cycles*, *21*(3). https://doi.org/10.1029/2007GB002923

Khatiwala, S. (2018). Version 2.0 of the transport matrix method software. https://doi.org/10.5281/ZENODO.1246300

Khatiwala, S. (2024). Transport matrix method code repository [Software]. *GitHub*. Retrieved from https://github.com/samarkhatiwala/tmm

Khatiwala, S., Schmittner, A., & Muglia, J. (2019). Air-sea disequilibrium enhances ocean carbon storage during glacial periods. *Science Advances*, *5*(6), eaaw4981. https://doi.org/10.1126/sciadv.aaw4981

Kohfeld, K. E., Graham, R. M., de Boer, A. M., Sime, L. C., Wolff, E. W., Le Quéré, C., & Bopp, L. (2013). Southern hemisphere westerly wind changes during the Last Glacial Maximum: Paleo-data synthesis. *Quaternary Science Reviews*, *68*, 76–95. https://doi.org/10.1016/j.quascirev.2013.01.017

Lambeck, K., Rouby, H., Purcell, A., Sun, Y., & Sambridge, M. (2014). Sea level and global ice volumes from the Last Glacial Maximum to the Holocene. *Proceedings of the National Academy of Sciences of the United States of America*, *111*(43), 15296–15303. https://doi.org/10.1073/PNAS.1411762111/SUPPL_FILE/PNAS.1411762111.SAPP.PDF

Lamy, F., Arz, H. W., Kilian, R., Lange, C. B., Lembke-Jene, L., Wengler, M., et al. (2015). Glacial reduction and millennial-scale variations in Drake Passage throughflow. *Proceedings of the National Academy of Sciences*, *112*(44), 13496–13501. https://doi.org/10.1073/pnas.1509203112

Large, W. G., & Yeager, A. S. G. (2022). The global climatology of an interannually varying air-sea flux data set. *Climate Dynamics*, *33*(2–3), 341–364. https://doi.org/10.1007/s00382-008-0441-3

Levitus, S., Antonov, J. I., Boyer, T. P., Baranova, O. K., Garcia, H. E., Locarnini, R. A., et al. (2012). World ocean heat content and thermosteric sea level change (0–2000 m), 1955–2010. *Geophysical Research Letters*, *39*(10). https://doi.org/10.1029/2012GL051106

Liang, J.-H., Deutsch, C., McWilliams, J. C., Baschek, B., Sullivan, P. P., & Chiba, D. (2013). Parameterizing bubble-mediated air-sea gas exchange and its effect on ocean ventilation. *Global Biogeochemical Cycles*, *27*(3), 894–905. https://doi.org/10.1002/gbc.20080

Lisiecki, L. E., & Stern, J. V. (2016). Regional and global benthic δ18O stacks for the last glacial cycle. *Paleoceanography*, *31*(10), 1368–1394. https://doi.org/10.1002/2016PA003002

Loose, B., & Jenkins, W. J. (2014). The five stable noble gases are sensitive unambiguous tracers of glacial meltwater. *Geophysical Research Letters*, *41*(8), 2835–2841. https://doi.org/10.1002/2013GL058804

Loose, B., Jenkins, W. J., Moriarty, R., Brown, P., Jullion, L., Naveira Garabato, A. C., et al. (2016). Estimating the recharge properties of the deep ocean using noble gases and helium isotopes. *Journal of Geophysical Research: Oceans*, *121*(8), 5959–5979. https://doi.org/10.1002/2016JC011809

Marcott, S. A., Bauska, T. K., Buizert, C., Steig, E. J., Rosen, J. L., Cuffey, K. M., et al. (2014). Centennial-scale changes in the global carbon cycle during the last deglaciation. *Nature*, *514*(7524), 616–619. https://doi.org/10.1038/nature13799

McGee, D., Broecker, W. S., & Winckler, G. (2010). Gustiness: The driver of glacial dustiness? *Quaternary Science Reviews*, *29*(17–18), 2340–2350. https://doi.org/10.1016/j.quascirev.2010.06.009

Moore, J. K., Abbott, M. R., Richman, J. G., & Nelson, D. M. (2000). The Southern Ocean at the Last Glacial Maximum: A strong sink for atmospheric carbon dioxide. *Global Biogeochemical Cycles*, *14*(1), 455–475. https://doi.org/10.1029/1999GB900051

Muglia, J., & Schmittner, A. (2015). Glacial Atlantic overturning increased by wind stress in climate models. *Geophysical Research Letters*, *42*(22), 9862–9868. https://doi.org/10.1002/2015GL064583

Pöppelmeier, F., Baggenstos, D., Grimmer, M., Liu, Z., Schmitt, J., Fischer, H., & Stocker, T. F. (2023). The effect of past saturation changes on noble gas reconstructions of mean ocean temperature. *Geophysical Research Letters*, *50*(6), e2022GL102055. https://doi.org/10.1029/2022GL102055

Rohling, E. J., Yu, J., Heslop, D., Foster, G. L., Opdyke, B., & Roberts, A. P. (2021). Sea level and deep-sea temperature reconstructions suggest quasi-stable states and critical transitions over the past 40 million years. *Science Advances*, *7*(26), eabf5326. https://doi.org/10.1126/sciadv.abf5326

Seltzer, A. (2024). UVic ESCM Pre-industrial and LGM simulations of inert gases in global ocean [Dataset]. *Zenodo*. https://doi.org/10.5281/zenodo.10402435

Seltzer, A. M., Ng, J., Aeschbach, W., Kipfer, R., Kulongoski, J. T., Severinghaus, J. P., & Stute, M. (2021). Widespread six degrees Celsius cooling on land during the Last Glacial Maximum. *Nature*, *593*(7858), 228–232. https://doi.org/10.1038/s41586-021-03467-6

Seltzer, A. M., Nicholson, D. P., Smethie, W. M., Tyne, R. L., Le Roy, E., Stanley, R. H. R., et al. (2023). Dissolved gases in the deep North Atlantic track ocean ventilation processes. *Proceedings of the National Academy of Sciences of the United States of America*, *120*(11), e2217946120. https://doi.org/10.1073/PNAS.2217946120/SUPPL_FILE/PNAS.2217946120.SD01.XLSX

Seltzer, A. M., Pavia, F. J., Ng, J., & Severinghaus, J. P. (2019). Heavy noble gas isotopes as new constraints on the ventilation of the deep ocean. *Geophysical Research Letters*, *46*(15), 8926–8932. https://doi.org/10.1029/2019GL084089

Shackleton, S., Baggenstos, D., Menking, J. A., Dyonisius, M. N., Bereiter, B., Bauska, T. K., et al. (2020). Global ocean heat content in the Last Interglacial. *Nature Geoscience*, *13*(1), 77–81. https://doi.org/10.1038/s41561-019-0498-0

Shackleton, S., Bereiter, B., Baggenstos, D., Bauska, T. K., Brook, E. J., Marcott, S. A., & Severinghaus, J. P. (2019). Is the noble gas-based rate of ocean warming during the younger dryas overestimated? *Geophysical Research Letters*, *46*(11), 5928–5936. https://doi.org/10.1029/2019GL082971

Shackleton, S., Seltzer, A., Baggenstos, D., & Lisiecki, L. E. (2023). Benthic δ18O records Earth's energy imbalance. *Nature Geoscience*, *16*(9), 1–6. https://doi.org/10.1038/s41561-023-01250-y

Sime, L. C., Hodgson, D., Bracegirdle, T. J., Allen, C., Perren, B., Roberts, S., & de Boer, A. M. (2016). Sea ice led to poleward-shifted winds at the Last Glacial Maximum: The influence of state dependency on CMIP5 and PMIP3 models. *Climate of the Past*, *12*(12), 2241–2253. https://doi.org/10.5194/cp-12-2241-2016

Sime, L. C., Kohfeld, K. E., Le Quéré, C., Wolff, E. W., de Boer, A. M., Graham, R. M., & Bopp, L. (2013). Southern hemisphere westerly wind changes during the Last Glacial Maximum: Model-data comparison. *Quaternary Science Reviews*, *64*, 104–120. https://doi.org/10.1016/j.quascirev.2012.12.008

Sueyoshi, T., Ohgaito, R., Yamamoto, A., Chikamoto, M. O., Hajima, T., Okajima, H., et al. (2013). Set-up of the PMIP3 paleoclimate experiments conducted using an Earth system model, MIROC-ESM. *Geoscientific Model Development*, *6*(3), 819–836. https://doi.org/10.5194/GMD-6-819-2013

Takahashi, T., Feely, R. A., Weiss, R. F., Wanninkhof, R. H., Chipman, D. W., Sutherland, S. C., & Takahashi, T. T. (1997). Global air-sea flux of CO2: An estimate based on measurements of sea–air pCO2 difference. *Proceedings of the National Academy of Sciences*, *94*(16), 8292–8299. https://doi.org/10.1073/pnas.94.16.8292

Tierney, J. E., Zhu, J., King, J., Malevich, S. B., Hakim, G. J., & Poulsen, C. J. (2020). Glacial cooling and climate sensitivity revisited. *Nature*, *584*(7822), 569–573. https://doi.org/10.1038/s41586-020-2617-x

Voldoire, A., Sanchez-Gomez, E., Salas y Mélia, D., Decharme, B., Cassou, C., Sénési, S., et al. (2013). The CNRM-CM5.1 global climate model: Description and basic evaluation. *Climate Dynamics*, *40*(9), 2091–2121. https://doi.org/10.1007/s00382-011-1259-y

Wang, P., Scott, J. R., Solomon, S., Marshall, J., Babbin, A. R., Lickley, M., et al. (2021). On the effects of the ocean on atmospheric CFC-11 lifetimes and emissions. *Proceedings of the National Academy of Sciences*, *118*(12), e2021528118. https://doi.org/10.1073/pnas.2021528118

Weaver, A. J., Eby, M., Wiebe, E. C., Ewen, T. L., Fanning, A. F., MacFadyen, A., et al. (2010). The UVic earth system climate model: Model description, climatology, and applications to past, present and future climates. *Atmosphere-Ocean*, *39*(4), 361–428. https://doi.org/10.1080/07055900.2001.9649686

Yokoyama, Y., Esat, T. M., Thompson, W. G., Thomas, A. L., Webster, J. M., Miyairi, Y., et al. (2018). Rapid glaciation and a two-step sea level plunge into the Last Glacial Maximum. *Nature*, *559*(7715), 603–607. https://doi.org/10.1038/s41586-018-0335-4

Yukimoto, S., Adachi, Y., Hosaka, M., Sakami, T., Yoshimura, H., Hirabara, M., et al. (2012). A new global climate model of the Meteorological Research Institute: MRI-CGCM3 —Model description and basic performance—. *Journal of the Meteorological Society of Japan. Ser. II*, *90A*(0), 23–64. https://doi.org/10.2151/jmsj.2012-A02

Zanna, L., Khatiwala, S., Gregory, J. M., Ison, J., & Heimbach, P. (2019). Global reconstruction of historical ocean heat storage and transport. *Proceedings of the National Academy of Sciences of the United States of America*, *116*(4), 1126–1131. https://doi.org/10.1073/PNAS.1808838115/SUPPL_FILE/PNAS.1808838115.SAPP.PDF

Zheng, W., & Yu, Y. (2013). Paleoclimate simulations of the mid-Holocene and last glacial maximum by FGOALS. *Advances in Atmospheric Sciences*, *30*(3), 684–698. https://doi.org/10.1007/s00376-012-2177-6